

Effective Star Formation Rates for Cosmological Applications

Marco Spaans¹

Harvard-Smithsonian Center for Astrophysics, 60 Garden Street, Cambridge, MA 02138

C. Marcella Carollo¹

Department of Physics & Astronomy, The Johns Hopkins University, Baltimore, MD 21218

ABSTRACT

Effective star formation rates in tabular form are computed which yield a prescription for the star formation activity in model galaxies as a function of ambient density, metallicity, and stellar feedback. The effects of supernova explosions on the thermal balance of the Interstellar Medium (ISM) and the presence of a multi-phase ISM are explicitly included. The resulting grid of models can be implemented easily in N-body codes for the computation of star formation processes in merging galaxies and cosmological simulations.

subject headings: galaxies: star formation - galaxies: structure - ISM - molecular processes

1. Introduction

The past decade has seen tremendous advances in the field of numerical cosmology (Navarro, Frenk & White 1996 and references therein). N-body simulations and hydro codes have benefitted from the large increase in CPU and memory capabilities of the current generation of supercomputers, and have reached a high enough sophistication to describe the development of large scale structure in the universe and the formation of galaxies with redshift. An important issue which ultimately needs to be addressed, in order to compare theory with observations of high redshift galaxies, is the formation of stars in proto-galactic structures (Norman & Spaans 1997, hereafter NS97, and references therein). Many parameterizations of the star formation rate in the ambient Interstellar Medium (ISM) exist in the literature and mostly derive from a Schmidt law applied to a sufficiently large body of gas (Theis et al. 1992; Kauffmann & White 1993; Spaans & Norman 1997, hereafter SN97).

Star formation is a local phenomenon which must find its explanation in the stability and fragmentation of dense molecular clouds. Studies in our own Galaxy have focussed on the structure of dense proto-stellar cores, along with the chemical and thermal balance of star-forming regions (Helmich 1996, and reference therein). These studies lend indirect support to a Schmidt law, but emphasize the need to include explicitly the structure of the multi-phase ISM to model accurately the most important heating and cooling processes. A large unknown in these investigations is the relative importance of feedback. Supernova explosions and stellar radiation associated with the process of star formation influence the global physical structure of the interstellar gas which supports this process.

Ideally, in the cosmological context one would like to solve for the properties of the thermal and chemical balance of the ISM and the star formation rate simultaneously with the solution of the gravitational

¹Hubble Fellow

N-body and hydrodynamical problem. Such an approach is beyond what is currently feasible and one is forced to decouple the ISM and star formation problem from the dynamical one. Along these lines, the purpose of this work is to present a set of numerical simulations which span a large range in density and metallicity, include a quantitative prescription for feedback, and yield the resulting star formation rate in the ambient medium in tabular form. This work extends the methods developed in a series of papers where the structure of the ISM and the importance of feedback effects have been investigated for proto-galactic disks (NS97), dwarf galaxies (SN97), massive proto-spheroidals in the Hubble Deep Field (Spaans & Carollo 1997), and elliptical galaxies (Carollo & Spaans 1998).

The strength of the procedure used in this work to produce the effective star formation rates is its detailed treatment of molecular line cooling, chemistry, and thermal balance (section 2) for a wide range of physical conditions. This allows for a detailed treatment of the multi-phase structure of the ambient ISM, and the feedback of stellar photons and supernova ejecta on its physical balance. The star formation rate is computed in our approach through a Schmidt law applied to the molecular phase of the ISM. The use of this empirical law presumes that star formation as observed in our local environment is representative of star formation in general. This seems a reasonable approach for spiral galaxies (Kennicutt 1989).

In the following sections, the input physics are discussed. The processes involved are complex, and various physical phenomena influence the final outcome of the computation. Therefore, one should keep the following major calculational steps in mind. 1) The thermal and chemical balance of the medium is determined locally and used to compute the amount of molecular gas. 2) This allows a calculation of the formation rate of stars according to a Schmidt law and an initial mass function (IMF). 3) The produced radiation is propagated across the computational grid in a radiative transfer calculation, and used to determine heating, ionization and dissociation rates. 4) The supernova blast waves, produced as the end products of stellar evolution, are propagated across the grid as well and yield the local input of kinetic (gas bulk motions) and thermal (gas heating) energy, as well as metals. 5) Steps 3 and 4 provide input for step 1. This entire procedure is followed for many different ambient densities, to derive the enrichment and physical state of the gas together with the corresponding star formation rate.

2. The Model: Stars Embedded in a Multi-Phase ISM

The models include three stellar and three gaseous components. The gas phases include the cold molecular clouds, the warm neutral/ionized medium, and the hot tenuous interiors of supernova bubbles. The phases are assumed to be in pressure equilibrium and their chemical and thermal balance is computed explicitly. The theoretical background for the evolution of the multi-phase ISM in primordial galactic structures is described in NS97 and SN97, where the employed numerical methods and a discussion of the spatial and temporal resolution of the adopted grid can also be found. Although no dynamics are included explicitly, there is mass exchange between the cold molecular and hot tenuous phase due to cloud evaporation. The density dependence for mass evaporation is given by $\propto E^{6/5} n_h^{-4/5}$, with E the supernova energy and n_h the density of the hot phase (McKee & Ostriker 1977). In the following we adopt for a grid cell a typical size of 20 pc, and time steps of 30-60 Myr. Even though we determine stationary solutions, it is necessary to integrate in time to determine the response of the ambient gas to the star formation process, i.e. stellar evolution, propagation of supernova shock waves etc.

The stellar components are divided according to their final evolutionary stages into massive stars of more than $11 M_\odot$, which explode as Type II supernovae, and low-mass stars, which are assumed to

lose their material in a planetary nebula phase. The low-mass stars will become $0.6 M_{\odot}$ white dwarfs (Weidemann & Koester 1983). Stars with masses below $0.6 M_{\odot}$ do not evolve during the lifetime of a galaxy. The third class of stars comprises the stellar remnants in the form of white dwarfs, neutron stars, and black holes. A fraction of the white dwarfs gives rise to Type Ia supernovae in the merging CO-dwarf picture (see below). Below we describe in detail the set of equations which are solved for the star formation (SF) and feedback processes: chemical and thermal balance, the occurrence and propagation of supernovae, metal yields and enrichment, radiative transfer, and stellar life cycles.

2.1. Star Formation

Following Larson (1991) the star formation rate is calculated with a Schmidt (1959) law applied to some volume in a galaxy with a gas mass M

$$\frac{\partial M_{\text{cm}}}{\partial t} = \alpha_{\text{SF}} \left(\frac{n_{\text{cm}}}{n_{\text{cm}}^0} \right)^b, \quad (1)$$

where the label “cm” indicates the cold molecular phase, n_{cm} is a number density, $n_{\text{cm}}^0 = 40 \text{ cm}^{-3}$ and $b = 1 - 2$. The coefficient α_{SF} is normalized to the SF rate as observed in molecular gas in the Solar vicinity

$$\alpha_{\text{SF}} = \frac{M}{M_{\text{g}}} \text{ M}_{\odot} \text{ yr}^{-1}, \quad (2)$$

with M normalized to the total body of gas M_{g} in the Milky Way (see below). For our own Galaxy as a whole this corresponds to an instantaneous rate of $\sim 3 M_{\odot} \text{ yr}^{-1}$ (Wyse 1997, private communication). The generic value of b is 1.3, but $b = 2$ is adopted in those low metallicity regions where the ambipolar diffusion time is shorter than the free-fall time of a molecular cloud (see NS97 for a detailed discussion).

The density of the cold molecular phase follows from application of the Field, Goldsmith, and Habing (1969) formalism to the thermal balance of a multi-phase ISM. The angular momentum of star-forming clouds is not included beyond the accuracy of the local Schmidt law applied to the cold molecular component. As such, we cannot address the (important) question of cloud fragmentation, and the IMF is an input parameter. We have assumed a time-independent Salpeter IMF $\phi(m) \propto m^{-2.35}$. Stellar masses between $0.1 M_{\odot}$ and $40 M_{\odot}$ are considered. It follows that approximately 10% of the newly formed stellar mass is incorporated into massive stars with a lifetime of no more 2×10^7 years.

2.2. Chemical Evolution

The evolutionary end stages of stars produce metals which provide most of the cooling (atomic and molecular lines) and dust opacity in a model galaxy. It is thus vital to know the production and spatial distribution of metallic species.

2.2.1. Elemental Abundances in the Gas Phase

The chemical evolution of elemental species has been discussed extensively in the literature, and the equations as described in Timmes, Woosley & Weaver (1995) and Tantaló et al. (1996) are adopted. The main difference with our implementation is the explicit three-dimensional spatial dependence of the chemical quantities. The treatment of physical processes is explicitly three-dimensional, and the spatial enrichment of the model galaxy through the expansion fronts of multiple supernovae is included. While the supernova bubble expands with time, the rate at which metals condense out into the cold molecular phase is computed to determine the local enrichment. The cooling rate of the enriched gas then determines whether a molecular phase can be supported, and at what interstellar gas density the SF process takes place. This eliminates the assumption of a one zone system. Although there is no infall of material, and the model galaxy is therefore a closed box, there is mass exchange (in particular metals) between the grid cells through the action of the SN expansion fronts.

For the stellar yields, three distinct components are specified: one for the massive stars ($11M_{\odot} \leq M \leq 40M_{\odot}$) which become Type II supernovae, one for the intermediate to low mass stars ($M \leq 11M_{\odot}$) which become planetary nebulae, and one for the remnants of the intermediate to low mass stars that become Type Ia supernovae (Timmes et al. 1995). The Type II supernova yields of Woosley & Weaver (1995) are adopted throughout. The yields from intermediate to low mass stars were taken from the CNO models with $1M_{\odot} \leq M \leq 8M_{\odot}$ of Renzini & Voli (1981). We have adopted their case B table for $Z = 0.004Z_{\odot}$ and $Z = Z_{\odot}$, and applied linear interpolation for the intermediate metallicities. For metallicities larger than Solar we extrapolated the yields linearly. This extrapolation does not strongly influence our results. By the time the ISM has been enriched to super-Solar metallicities, most of the baryons in a model galaxy have been incorporated into stars. The W7 model of Nomoto, Thielemann & Yokoi (1984) was adopted for the Type Ia supernovae.

The average mass $\xi_i(p, t)$ and abundance $X_i(p, t)$ of the elemental species in a grid cell centered on the point $p = (x, y, z)$ at time t are governed by

$$\begin{aligned} \frac{d\xi_i(p, t)}{dt} = & -X_i(p, t)S(p, t) + \int_{M_{\min}}^{m_B} S(p, t - t_M)Y_{M,i}(t - t_M)I(M)dM + \\ & C \int_{m_B}^{M_B} I(M) \left[\int_{\mu_{\min}}^{0.5} f(\mu)S(p, t - t_{M_2})Y_{M,i}(t - t_{M_2})d\mu \right] dM + \\ & (1 - C) \int_{m_B}^{M_B} S(p, t - t_M)Y_{M,i}(t - t_M)I(M)dM + \\ & \int_{M_B}^{M_{\max}} S(p, t - t_M)Y_{M,i}(t - t_M)I(M)dM. \end{aligned} \quad (3)$$

In the equation, $S(p, t)$ is the normalized SF rate, $Y_{M,i}$ are the elemental yields of elements i from stars of mass M , $I(M)$ is the initial mass function whose lower and upper limits are M_{\min} and M_{\max} , t_M is the lifetime of a star of mass M , and t_{M_2} is the lifetime of the secondary in the binary, which determines the time required for the system to undergo a Type Ia event. In the models this lifetime depends on the initial chemical composition as tabulated in Bertelli et al. (1994). The various integrals which appear in Equation (3) represent the contributions of Type II and Type Ia supernovae in the formulation of Matteucci & Greggio (1986). Specifically, the second integral reflects those binary systems which have the necessary properties to produce Type Ia supernovae, m_B and M_B are the lower and upper mass limit for the total mass of the binary system, $f(\mu)$ is the distribution function of their mass ratios, and μ_{\min} denotes the minimum value of this ratio. The lower integration limit is equal to $3 M_{\odot}$, to ensure that the accreting

white dwarf can reach the Chandrasekhar limit. The upper mass limit is equal to $16 M_{\odot}$ for a binary system, based on the assumption that the maximum mass of the primary that produces a carbon-oxygen white dwarf is $8 M_{\odot}$. The constant C indicates which fraction of all binary systems undergo supernova events. This constant is chosen equal to $C = 0.007$ to reproduce the solar ^{56}Fe abundance (Timmes et al. 1995).

2.2.2. Atomic and Molecular Species

If one knows the local elemental abundances and the radiation field (discussed below) then it is possible to determine the chemical composition of the ambient gas. To derive the abundances of atomic and molecular species, the solution vector of a chemical network in point p is computed according to

$$H(T(p), n_i(p)) = \frac{dn_i(p)}{dt} = 0. \quad (4)$$

Here H denotes the chemical network, T is the ambient temperature, and the chemical abundances by number n_i are determined in steady state. That is, the evolution time of a galaxy, a free-fall time ~ 500 Myr, is assumed to be long compared to the time to reach chemical equilibrium, ~ 50 Myr for diffuse H_2 gas and much shorter for all other molecular species. Only in a very low metallicity environment, $Z \sim 0.005 Z_{\odot}$, is the formation time scale of H_2 as long as 500 Myr and intimately linked to the dynamical evolution of the system.

The adopted reaction network is based on that used by van Dishoeck & Black (1986, 1989) to model the chemistry of translucent clouds, combined with the sulfur chemistry as described in Drdla et al. (1989). The network has been checked against the UMIST database (Millar et al. 1991), and only minor differences have been found. The chemical network includes 24 elements, and isotopes of H, C and O. The inclusion of many metals is important because they dominate the ionization balance and differences in ionization potential become important for extinctions of more than 2 mag. The network includes 1549 reactions among 215 species. We adopt the line and continuum photo-dissociation cross sections based on the literature summarized by van Dishoeck (1988).

2.3. Thermal Balance

The heating of the ISM involves radiative sources like stars as well as mechanical sources like stellar winds and supernova expansion fronts. Cooling is provided by line emission from hydrogen and metallic ions as well as continuum processes. In order to determine the thermal state of the gas, one needs to find the solutions (ρ, T) of the fundamental energy (E) equation

$$\frac{dE(T, \rho, t)}{dt} = \Gamma(T, \rho, t) - \Lambda(T, \rho, t). \quad (5)$$

In this equation, T is the temperature, ρ is the gas density, Γ is the total heating rate and Λ the total cooling rate, both per unit of mass. In the following subsections the various terms which contribute to the overall balance are discussed.

2.3.1. Heating by Supernovae

The hydrodynamics of interstellar gas is not treated explicitly in our work, and the results of various numerical studies are used to implement the contribution from mechanical processes such as supernova blast waves. We adopt the formulations of Bertelli et al. (1994) for Type II, and of Greggio & Renzini (1983) for Type Ia supernovae. The total energy injection due to supernovae of Type X which last for a time Δt is given by

$$\Gamma_X = \int_{\Delta t} \epsilon_X(t-t')R_X(t')dt', \quad (6)$$

where $R_X(t)$ is the number of supernovae per unit mass and time, and $\epsilon_X(t)$ describes the thermalization of the supernova energy as a function of time when cooling effects are properly taken into account. For ϵ_X we adopt the results of Gibson (1995) and Thornton et al. (1997). From the latter authors we adopt the radial evolution of the supernova remnants to determine the distribution of metal-rich tenuous gas as it condenses out into the cold molecular phase. The rate R_X is computed from the local star formation rate in grid point p at time t and depends on the assumed IMF. We have also included in Equation (5) the work performed by supernova shocks through the acceleration of molecular clouds. From Thornton et al. (1997) we take the fraction of the initial supernova explosion energy which ends up as kinetic energy of the ISM.

2.3.2. Heating by Stellar Winds

The rate of energy injection by stellar winds has a similar form, namely:

$$\Gamma_W = \int_{\Delta t} \epsilon_W(t-t')R_W(t')dt', \quad (7)$$

where $R_W(t)$ is the number of stars per unit mass and time expelling their envelopes during the time interval Δt . The quantity ϵ_W has the same meaning as ϵ_X . A star which is shedding mass, deposits an energy of (Gibson 1994)

$$\epsilon_{W0} = 0.15M_{ej}(M)(Z/Z_\odot)^{0.75}v(M)^2, \quad (8)$$

where M_{ej} is the amount of mass ejected by a star of mass M and $v(M)$ is the velocity of the ejected material. The velocity $v(M)$ is assumed to be equal to the maximum of the terminal velocity of the wind $\approx 20 \text{ km s}^{-1}$ or the galaxy velocity dispersion. The adopted process of thermalization is as described in Bertelli et al. (1994). The magnitude of this heating source is not that accurately known, but it does not dominate the thermal balance of the ISM.

2.3.3. Heating by Ultraviolet Photons

The ionization heating and charge balance of the medium is explicitly included through the Saha equation applied to H, He, C, O, N, S, Fe, Si, and Mg. The energy density and shape of the radiation field follows from

$$E_{UV} = \int_{\Delta t} \epsilon_{UV}(t-t')R_{UV}(t')dt', \quad (9)$$

where all the symbols have their usual meaning. In the determination of ϵ_{UV} we use the stellar population models of Leitherer et al. (1996) for a Salpeter IMF.

To assess which fraction of the ultraviolet energy is available for heating, ionization and dissociation, a continuum radiative transfer calculation is required. In the literature (Granato et al. 1997 and references therein) one finds a typical number of 0.01 for the fraction of the ultraviolet light which is not absorbed by dust and re-radiated as infrared radiation. Because the abundances of metals and therefore of dust may vary strongly across the galaxy, the Monte Carlo radiative transfer method of Spaans (1996) is adopted to compute the strength of the average radiation field from the SF rate and the local metallicity (SN97). The star formation rate used in the radiative transfer computation is a local average over a grid cell, and yields a local source function for the ultraviolet radiation field. This way local fluctuations in the radiation field strength are taken into account in the chemical and thermal balance.

For the molecular phase with metallicities larger than 1% of Solar, the dominant heating mechanism is the emission of photo-electrons from dust grains. The formalism of Bakes & Tielens (1994) is adopted with the implementation as described in Spaans et al. (1994). Part of the photo-electric heating of the molecular ISM is provided by large molecules like PAHs (polycyclic aromatic hydrocarbons), and their abundance is assumed to be equal to 10% of the gas phase carbon.

2.3.4. Heating by Proto-Galactic Collapse

Since the purpose of the effective SF rates is to study the gas phase processes during the formation of galaxies, we also include the heating which results from the infall of material on a time scale τ_{ff} and leads to the formation of the galaxy (Binney & Tremaine 1987). This is an aspect of our calculations where a coupling with realistic gas dynamics from a cosmological formalism would be most desirable. Decoupling the ISM from the dynamics, we adopt a simplified approach here. If R_i is the initial radius of the proto-galaxy, then

$$\tau_{\text{ff}} = \pi \sqrt{\frac{R_i^3}{2GM}}, \quad (10)$$

where M is the total mass of the galaxy. If no other energy sources are present, a proto-galactic cloud at the virial temperature cools on a time scale

$$\tau_{\text{cool}} = 6.3 \times 10^5 (R_i/10\text{kpc})^2 \quad \text{yr}. \quad (11)$$

At the end of the collapse phase the system is assumed to have an energy given by

$$E_{\text{vir}} = E_{\text{vir},0} \left(1 - \frac{\tau_{\text{cool}}}{\tau_{\text{ff}}}\right), \quad (12)$$

where $E_{\text{vir},0}$ is the initial virial energy. The remaining energy at the end of the collapse phase is converted into heat at the rate

$$\Gamma_{\text{c}} = \frac{E_{\text{vir}}}{\tau_{\text{ff}}}. \quad (13)$$

This source of heating remains active as long as the age of the galaxy is less than τ_{ff} , and sets the initial gas temperature. The latter is very important for the early low metallicity chemical balance which pertains in the primordial gas. We adopt a collapse factor $\lambda \approx 30$ (NS97), i.e. $R_i \sim 300$ kpc.

2.3.5. *Relative Importance of Heating Processes and Galactic Winds*

As mentioned above, the heating of the molecular gas is dominated by photo-electric emission for metallicities in excess of $0.01Z_{\odot}$. It is this rate which determines to a large extent the thermal and chemical balance of the multi-phase ISM, and therefore the effective star formation rate supported by the ambient molecular gas. Nevertheless, the other heating terms are of importance as well during certain epochs. The proto-galactic collapse phase provides the initial thermal structure of the ambient gas prior to the formation of stars. It thus fixes the chemical abundances of the primordial galaxy. During periods of massive star formation, the energy input from supernovae becomes comparable or even larger than the photo-electric heating rate in small regions of the galaxy where the supernova blast wave interacts with the ambient interstellar gas.

If the supernova energy input dominates during some period of time, the temperature or kinetic energy of the interstellar gas can increase and may become comparable to the gravitational binding energy of the model galaxy. In this case a wind develops which is assumed to quench the SF process (e.g. Larson 1974; Carlberg 1984; Arimoto & Yoshii 1987; Matteucci & Tornambé 1987; De Young & Heckman 1991).

2.4. **Cooling by Line and Continuum Processes**

The cooling rate depends crucially on the abundance of certain atoms and molecules like C, O, H₂ and CO, and the ability for radiation to escape from the medium, i.e. radiative transfer. For temperatures above 10^4 K, the metallicity dependent tabulations of Sutherland & Dopita (1993) and the cooling curves of Ferrara (1996, private communication) are adopted. For these high temperatures the cooling is dominated by thermal bremsstrahlung and by atomic hydrogen around 10^4 K. Unlike other treatments (Chiosi et al. 1997) we do not use cooling functions below 10^4 K, but solve the statistical equilibrium and the radiative transfer problem explicitly (Spaans & van Dishoeck 1997; SN97).

The fine-structure lines of C⁺, C, O, Si⁺, Si, S⁺, S, Fe⁺, and Fe are included, as well as the rotational lines of CO and H₂. The vibrational excitation of the latter molecule is also included. The thermal balance of the molecular phase strongly depends on the chemistry and thereby influences the effective SF rate of the interstellar gas. A detailed treatment of optical depth effects in the cooling lines is therefore required to determine the various densities and temperatures of the components of the multi-phase ISM (NS97). Note that in redshift dependent calculations, the temperature of the Cosmic Microwave Background (CMB) should be taken explicitly into account for redshifts larger than 5. The latter effect is of particular importance for the excitation of CO molecules, and influences the effective cooling rate of molecular gas (Silk & Spaans 1997). Still, we do not expect the effective star formation rate to change much and the application of our results is likely to be to lower redshift objects. Therefore we have considered only a 3 K CMB.

3. **Results and Discussion**

3.1. **Model Characteristics**

In the computation of the star formation rates, the total body of gas simulated is $M_g = 10^{10} M_\odot$, i.e. the gas mass of the Milky Way. The effective star formation rates presented here should be scaled linearly when implemented in dynamical simulations with some mass resolution element M_{res} . To model the effect of outflows on the star formation process the body of gas is assumed to be embedded in a $M_{\text{pot}} = 5 \times 10^{11} M_\odot$ spherical potential with a r^{-2} density profile outside a constant density core (Spaans & Carollo 1997). The energy estimates of SN97 are used to determine when the gas becomes unbound and star formation is quenched. We have assumed a generic SN kinetic energy of 10^{51} ergs, and that 10% of the initial SN energy ends up as turbulent kinetic energy of the interstellar clouds. The amount of kinetic energy transferred from the SN expansion front to the ISM is not that well determined. Nevertheless, recent one-dimensional numerical simulations by Thornton et al. (1997) indicate that 10% is a reasonable value. The value of M_{pot} determines the binding energy of the gas in a linear fashion. The maximum possible star formation rate, i.e. when a galactic wind does not yet develop, therefore scales with M_{pot} in our formalism. This scaling does not take into account the nature of the outflow which develops for a galaxy with a specific density profile. If the potential is not static the local density changes should be well captured by our formalism (barring shocks). The maximum star formation rate on the other hand would change, and our method does not accurately capture these effects.

The characteristic time scale and absolute rate of star formation depend on the thermal and chemical balance of the ISM. For the numerical simulations presented here, a grid was set up in parameter space which includes total hydrogen number densities $n_H = 10^{-2} - 10^6 \text{ cm}^{-3}$ and metallicities $Z = 5 \times 10^{-3} - 3 Z_\odot$. The locally produced stellar radiation field and the input of kinetic and thermal energy by supernova explosions render our equation for the local star formation rate non-linear due to feedback effects. The numerical simulations have therefore been performed for a range of “background” SF rates $S_b = 0.3 - 300 M_\odot \text{ yr}^{-1}$. The SF rates at the low end of the background range can be much larger than $300 M_\odot \text{ yr}^{-1}$ initially, but as S increases, feedback effects in the form of outflows limit the sustained SF rate to $\sim 10^3 M_\odot \text{ yr}^{-1}$. This result depends on the adopted values of M_g and M_{pot} as discussed above. In practical applications, the background star formation rate should be defined by neighboring grid cells or a previous time step.

3.2. Physical Processes

Before turning to the specific results, it is good to bear in mind the following physical processes which determine to a large extent the conclusions of this paper. For metallicities of less than a percent of Solar, the chemistry is dominated by H, He, Li, their ions, H^- , and molecules like H_2 and HD. The latter two, together with atomic hydrogen, provide the cooling of the ambient gas. The dominant formation route of H_2 involves the H^- radical rather than dust grains. A consequence, of importance for the results presented here, is that star formation is a global process. That is, the lack of dust allows stellar UV photons to traverse throughout the medium almost unattenuated and to influence the physical structure of the ISM over very large distances. In NS97 it is shown that this mode of star formation is self-regulating due to the strong dependence of the H^- abundance on the radiation field strength shortward of 912 \AA , and the fact that H_2 is only dissociated by photons longward of 912 \AA . The typical H_2 driven star formation rate for a proto-galactic disk is small and of the order of $0.01\text{-}0.1 M_\odot \text{ yr}^{-1}$. The relevance of this number for low surface brightness galaxies will be discussed in a forthcoming paper (Spaans, Mihos, & McCaugh 1998; in preparation).

For metallicities in excess of a few percent of Solar, the above picture changes dramatically. The presence of metallic atoms enhances the cooling rate and allows the formation of molecules like OH, H₂O and CO. Also the formation of H₂ proceeds much more efficiently on the surfaces of dust grains. Due to the increased dust opacity, the formation of stars is a local process. Stellar photons are absorbed close to the source and the presence of metallic atoms and molecules allows a large fraction of this input energy to be radiated away efficiently.

The following phases can then be distinguished in the evolution of the ambient medium: Only a small fraction of baryonic matter is converted into stars due to H₂ and HD cooling in a very low metallicity medium. The regions where the H₂ abundance is large are characterized by a kinetic temperature of ~ 1000 K, due to vibrational line cooling, and an ambient pressure of 2×10^3 K cm⁻³. The efficient formation of stars begins with a transition to a multi-phase ISM at 5×10^3 K cm⁻³, which includes cold molecular clouds. This transition occurs at a metallicity of the order of $\sim 0.03Z_{\odot}$. The multi-phase ISM is able to cool away most of the UV stellar photons through infrared lines and dust continuum emission.

3.3. Model Results

Figure 1 presents the general dependence on metallicity and hydrogen number density (for a mass M_g) and a background star formation rate $S_b = 3 M_{\odot} \text{ yr}^{-1}$. The dots in Figure 1 (and Figure 2) indicate individual entries in Table 1. Note here that the model results presented in Table 1 have been interpolated with a low order polynomial to create a grid which is homogeneous in both density and metallicity. Around the threshold metallicity of $\sim 0.03 Z_{\odot}$, the sustained SF rate is a strong function of the ambient enrichment. Because the cooling rate cannot keep up with the ambient heating, a small rise in the SF rate raises the temperature of the ISM to above ~ 1000 K where H₂ is collisionally destroyed. Conversely, a small increase in metallicity increases both the cooling and the H₂ formation rate on dust grains, and therefore the sustained SF rate. Once a multi-phase ISM has been firmly established for metallicities roughly within an order of magnitude of Solar, the star formation rate does not vary with metallicity by more than a factor of two. This relative insensitivity to metallicity in a multi-phase ISM is due to the ability of the gas to cool through infrared line transitions and dust emission.

Note that the 0.01 and $0.02Z_{\odot}$ curves are the same for number densities below 0.03 cm^{-3} , but not the same as the 0.005 and $0.05Z_{\odot}$ curves below that number density. Below a metallicity of $\sim 0.01Z_{\odot}$, a multi-phase ISM does not exist. The $0.005Z_{\odot}$ curve therefore pertains to a medium cooled predominantly by H, H₂ and HD. Conversely, for metallicities close to the phase transition, but at low densities, the pressure-density curve which determines the phase structure of the ambient gas, does not vary much with metallicity. This is caused by the fact that for these parameters the heating and cooling rates vary proportionally.

Figures 1 and 2 also illustrate the importance of feedback to limit the global SF rate to no more than $\sim 10^3 M_{\odot} \text{ yr}^{-1}$ for the masses and ambient densities considered here. A system with ($M_{\text{pot}} = 5 \times 10^{11} M_{\odot}$, $M_g = 10^{10} M_{\odot}$) starts to unbound its ISM kinematically for a star formation rate of $\sim 10^3 M_{\odot} \text{ yr}^{-1}$, even though the thermal energy contributed to the molecular ISM can be largely radiated away through line and dust emission. This causes a break in the star formation rate with density for a given metallicity. For low densities and SF rates the slopes in Figures 1 and 2 are for a large part dictated by the assumed Schmidt law. This limit to the star formation rate should be indicative for the formation of L^* -type galaxies,

and appears to be in agreement with current results for the Hubble Deep Field (Madau et al. 1996). A dynamical implementation of our results will yield a more accurate determination of these effects since they could account for re-accretion and the extent of the dark matter potential.

It is good to take note of the time scales to reach chemical equilibrium in media of varying metallicity. For a low metallicity environment of 0.5 percent of Solar, the time to reach chemical equilibrium for the H_2 abundance in a cloud of 100 cm^{-3} is approximately 500 Myr for a background radiation field of 0.1 in units of J_{-21} . In the multi-phase ISM the corresponding time scale is a bit less than 20 Myr. It is the H_2 abundance which provides the initial cooling and drives the ion-molecule chemistry required for the formation of molecules like OH, CH, H_2O , CO etc. The decrease in this time scale with metallicity therefore gives a direct measure of the efficiency with which stars can be formed.

These time scales are also relevant to the blow-out phenomenon in flattened galaxies. A supernova shock front originating from the disk of a galaxy and travelling at 100 km s^{-1} will reach a height of 1 kpc in 10 Myr. This time scale is of the same order as the chemical equilibrium time as well as the cooling time of the gas. The hot metal-rich cavity gas therefore does not have enough time to cool and form (molecular) clouds which are more robust and could help to retain the metals, even in a multi-phase ISM (Spaans & Carollo 1997).

3.4. Sensitivity to Model Assumptions and Parameters

Some of the numbers which go into the calculation have a large influence on the final result and are also poorly determined. These will be discussed below.

1) An optimal metallicity range of $\sim 0.04 - 0.2Z_\odot$ seems to exist, for which SF can proceed more efficiently at high densities (SN97). This effect is due to the absence of magnetic support for low metallicity molecular clouds. A low ionization fraction yields an ambipolar diffusion time scale which is shorter than the free-fall time of a molecular cloud. The calculations presented here limit this increase in the SF rate to about of factor of two due to the grain chemistry adopted at high extinction. Deep inside molecular clouds grains are predominantly neutral and provide an important sink for the free electrons followed by rapid recombination with (metallic) ions (Lepp & Dalgarno 1988). This leads to a medium with a higher fractional ionization compared to the case where electron recombination dominates. The rates for these processes are typically $10^{-6} \text{ cm}^3 \text{ s}^{-1}$, but are not accurately known due to their dependence on the grain size distribution. Additional calculations at a selected number of densities which involve a chemical network with more detailed charge transfer effects and exchange rates larger by a factor of three, indicate that the star formation rates in the optimal metallicity range may be larger by about 100%. The more conservative estimates are retained here because only cloud collapse models could provide a definite answer. These seem to indicate that diffusion of the magnetic field aids the formation of stars, but is not a sufficient condition by itself (Gammie 1997, private communication).

2) Related to the issue of molecular clouds at high visual extinctions, is the matter of grid resolution. The implemented method allows the gas to be resolved down to the 20 pc level, i.e. individual molecular clouds. Any increase in grid resolution is therefore not expected to change our results. Still, the star formation process itself involves the fragmentation of molecular cloud cores and smaller scales should therefore be probed to put the adopted Schmidt star formation law on a firmer basis. Such an increase in resolution must be accompanied by a hydrodynamic treatment of the gas to accurately model for instance

the effects of shocks. The latter are very dissipative phenomena and strongly influence the thermal balance of the ambient gas. It is expected that in a high metallicity medium, molecules will be (re-)formed efficiently in the shock’s wake. Therefore, the energy will be efficiently radiated away in the form of long wavelength photons and the gas can condense to high densities. This will increase the effective star formation rate, although the magnitude of the effect lies beyond the scope of the present work.

3) The heating rate due to supernova explosions can become comparable to the UV heating rate in some parts of the model galaxy. Nevertheless, the former number is not accurately known and we have therefore run models where the thermalized fraction of the input supernova energy is a factor of 5 larger. For low metallicities in a H_2 cooling dominated medium, the temperature of the gas rises with a factor of a few, from ~ 1000 to ~ 4000 K. This increases the collisional destruction rate of molecular hydrogen, the dominant coolant, and therefore inhibits further star formation. Once a multi-phase ISM has been established, the ambient gas is capable of radiating away the extra input energy efficiently and the results for the star formation rates do not change by more than 30-50%.

4) We have ignored the contribution from Type Ib supernovae. It appears that radiative stellar winds from massive stars may be significantly suppressed at low metallicities, but that winds driven by binary star evolution could increase the number of Type Ib supernovae in the early universe (Timmes 1998, private communication). Such an effect could increase the relative abundance of oxygen. Since atomic oxygen is an important coolant and strongly influences the chemistry of OH and CO, our results potentially can be altered by a higher Type Ib supernova rate. For a higher oxygen production rate of a factor of three, it turns out that the cooling rate due to [OI] is not strongly influenced because the main cooling line, [OI] $63 \mu\text{m}$, is optically thick. The abundance of CO is favorably increased and the molecular phase can cool more efficiently. For the adopted factor of three, the star formation rate maximally increases by 40%.

If one combines the uncertainties 1-4, it appears that the magnitude of the star formation rates presented here can change by at most a factor of four, and are typically accurate to a factor of two. We feel that the existence of a threshold metallicity, as depicted in Figures 1 and 2, is quite robust since it derives from a detailed treatment of the thermal balance of the ISM for a range of background radiation fields.

4. Conclusions

We have derived star formation rates in tabular form as functions of the ambient density, metallicity, and stellar feedback in proto-galaxies with a given total gas mass. We have explicitly included the effects of supernova explosions on the thermal balance of the ISM, and the transition to a multi-phase ISM. The strength of the method used to produce the effective star formation rates is the detailed treatment of molecular line cooling, chemistry, and thermal balance. The tabulated star formation rates can be implemented in N-body codes for the computation of star formation processes in merging galaxies and cosmological simulations. The accuracy of the presented numbers is expected to be of the order of a factor of two, and in any case the rates should not change by more than a factor of four. The full set of numerical results is included in Table 1, and can be obtained in machine readable form from MS.

Although we have included the effects of feedback self-consistently, the present calculations cannot capture the effects of massive shocks associated with a large collection of SN explosions propagating through the ISM. A complete treatment of the latter requires the incorporation of the numerical scheme adopted here in a full hydro treatment. Investigations along these lines are being pursued.

The authors are grateful to Colin Norman and Frank Timmes for stimulating comments. MS and CMC are supported by NASA through grants HF-01101.01-97A and HF-1079.01-96a, respectively, awarded by the Space Telescope Institute, which is operated by the Association of Universities for Research in Astronomy, Inc., for NASA under contract NAS 5-26555.

REFERENCES

- Arimoto, N., & Yoshii, Y. 1987, *A&A*, 173, 23
- Bakes, E.L.O., & Tielens, A.G.G.M. 1994, *ApJ*, 427, 822
- Bertelli, G., Bressan, A., Chiosi, C., Fagotto, F., & Nasi, E. 1994, *A&AS*, 106, 275
- Binney, J.J., & Tremaine, S. 1987, *Galactic Dynamics*, Princeton University Press, NJ
- Carlberg, R.C. 1984, *ApJ*, 286, 403
- Carollo, C.M., & Spaans, M. 1998, in preparation
- Chiosi, C., Bressan, A., Portinari, L., & Tantalo, R. 1997, *A&A* in press
- Drdla, K., Knapp, G.R., & van Dishoeck, E.F. 1989, *ApJ*, 345, 815
- Field, G.B., Goldsmith, D., & Habing, H.J. 1969, *ApJ*, 155, L149
- Gibson, B.K. 1994, *MNRAS*, 271, 35
- Gibson, B.K. 1995, PhD Thesis, University of British Columbia, Canada
- Granato, G.L., Silva, L., Danese, L., Bressan, A., Franceschini, A., & Chiosi, C. 1997, *ESA First Symposium* 401, in press
- Greggio, L., & Renzini, A. 1983, *A&A*, 118, 217
- Helmich, F.P., 1996, Ph.D. thesis Leiden
- Kauffmann, G., & White, S.D.M. 1993, *MNRAS*, 261, 921
- Kennicutt, R.C. 1989, *ApJ*, 344, 685
- Larson, R.B. 1974, *MNRAS*, 166, 385
- Larson, R.B. 1991, in *Frontiers of Stellar Evolution*, ed. D.L. Lambert, ASP Conf. Ser. 20, 571
- Leitherer, C., et al. 1996, *PASP*, 108, 996
- Lepp, S., & Dalagarno, A. 1988, *ApJ*, 324, 553
- Madau, P., Ferguson, H.C., Dickinson, M.E., Giavalisco, M., Steidel, C.C., & Fruchter, A. 1996, *MNRAS*, 283, 1388
- Matteucci, F., & Greggio, L. 1986, *A&A*, 154, 279
- Matteucci, F., & Tornambé, A. 1987, *A&A*, 185, 51
- McKee, J.F., & Ostriker, J.P. 1977, *ApJ*, 218, 148
- Millar, T.J., Bennet, A., Rawlings, J.M.C., Brown, P.D., & Charnley, S.B. 1991, *A&AS*, 87, 585
- Navarro, J.F., Frenk, C.S., & White, S.D.M. 1996, *ApJ*, 462, 563

- Nomoto, K., Thielemann, F.K., & Yokoi, K. 1984, *ApJ*, 286, 684
- Norman, C.A., & Spaans, M. 1997, *ApJ*, 480, 145 (NS97)
- Renzini, A., & Voli, M. 1981, *A&A*, 94, 175
- Schmidt, M. 1959, *ApJ*, 129, 243
- Silk, J., & Spaans, M. 1997, *ApJ*, 488, L79
- Spaans, M. 1996, *A&A*, 307, 271
- Spaans, M., Tielens, A.G.G.M., van Dishoeck, E.F., & Bakes, E.L.O. 1994, *ApJ*, 437, 270
- Spaans, M., & van Dishoeck, E.F. 1997, *A&A*, 323, 953
- Spaans, M., & Norman, C.A. 1997, *ApJ*, 488, 27 (SN97)
- Spaans, M., & Carollo, C.M. 1997, *ApJ*, 482, L93
- Sutherland, R.S., & Dopita, M.A. 1993, *ApJS*, 88, 253
- Tantalo, R., Chiosi, C., Bressan, A., & Fagotto, F. 1996, *A&A*, 311, 361
- Theis, C.H., Burkert, A., & Hensler, G. 1992, *A&A*, 265, 465
- Thornton, K., Gaudlitz, M., Janka, H.-Th., & Steinmetz, M. 1997, *astro-ph/9706175*
- Timmes, F.X., Woosley, S.E., & Weaver, T.A. 1995, *ApJS*, 98, 617
- van Dishoeck, E.F. 1988, in *Rate Coefficients in Astrochemistry*, eds. T.J. Millar & D.A. Williams, Kluwer, Dordrecht, p. 49
- van Dishoeck, E.F., & Black, J.H. 1986, *ApJ*, 307, 332
- van Dishoeck, E.F., & Black, J.H. 1989, *ApJ*, 340, 273
- Weidemann, V., & Koester, D. 1983, *A&A*, 121, 77
- Woosley, S.E., & Weaver, T.A. 1995, *ApJS*, 101, 181

Table 1
 Effective Star Formation Rates (SF) as Functions of Metallicity,
 Background Star Formation Rate (BSF) and Density

Z/Z_{\odot}^b	$n_{\text{H}} \text{ (cm}^{-3}\text{)}^b$	SF ^a	BSF ^a	SF	BSF	SF	BSF	SF	BSF
5.00E-03	1.00E-02	0.01	0.30	0.01	3.00	0.01	30.0	0.01	300.0
5.00E-03	2.00E-02	0.01	0.30	0.01	3.00	0.01	30.0	0.01	300.0
5.00E-03	5.00E-02	0.03	0.30	0.01	3.00	0.01	30.0	0.01	300.0
5.00E-03	1.00E-01	0.10	0.30	0.04	3.00	0.01	30.0	0.01	300.0
5.00E-03	2.00E-01	0.13	0.30	0.10	3.00	0.01	30.0	0.01	300.0
5.00E-03	5.00E-01	0.19	0.30	0.12	3.00	0.02	30.0	0.01	300.0
5.00E-03	1.00E-00	0.40	0.30	0.21	3.00	0.06	30.0	0.01	300.0
5.00E-03	2.00E-00	0.62	0.30	0.39	3.00	0.10	30.0	0.01	300.0
5.00E-03	5.00E-00	0.81	0.30	0.58	3.00	0.13	30.0	0.01	300.0
5.00E-03	1.00E+01	0.99	0.30	0.67	3.00	0.19	30.0	0.02	300.0
5.00E-03	2.00E+01	1.10	0.30	0.84	3.00	0.31	30.0	0.03	300.0
5.00E-03	5.00E+01	1.42	0.30	0.98	3.00	0.41	30.0	0.05	300.0
5.00E-03	1.00E+02	1.74	0.30	1.19	3.00	0.55	30.0	0.09	300.0
5.00E-03	2.00E+02	1.96	0.30	1.30	3.00	0.69	30.0	0.12	300.0
5.00E-03	5.00E+02	2.11	0.30	1.49	3.00	0.81	30.0	0.19	300.0
5.00E-03	1.00E+03	2.40	0.30	1.60	3.00	0.93	30.0	0.24	300.0
5.00E-03	2.00E+03	2.61	0.30	1.84	3.00	1.08	30.0	0.30	300.0
5.00E-03	5.00E+03	2.80	0.30	1.98	3.00	1.20	30.0	0.41	300.0
5.00E-03	1.00E+04	2.93	0.30	2.12	3.00	1.39	30.0	0.51	300.0
5.00E-03	2.00E+04	3.04	0.30	2.31	3.00	1.54	30.0	0.62	300.0
5.00E-03	5.00E+04	3.12	0.30	2.43	3.00	1.67	30.0	0.73	300.0
5.00E-03	1.00E+05	3.24	0.30	2.75	3.00	1.85	30.0	0.81	300.0
5.00E-03	2.00E+05	3.36	0.30	2.89	3.00	1.98	30.0	0.90	300.0
5.00E-03	5.00E+05	3.41	0.30	2.96	3.00	2.12	30.0	0.99	300.0
5.00E-03	1.00E+06	3.50	0.30	3.03	3.00	2.23	30.0	1.08	300.0
1.00E-02	1.00E-02	0.10	0.30	0.10	3.00	0.10	30.0	0.10	300.0
1.00E-02	2.00E-02	0.10	0.30	0.10	3.00	0.10	30.0	0.10	300.0
1.00E-02	5.00E-02	0.13	0.30	0.10	3.00	0.10	30.0	0.10	300.0
1.00E-02	1.00E-01	0.19	0.30	0.12	3.00	0.10	30.0	0.10	300.0
1.00E-02	2.00E-01	0.28	0.30	0.19	3.00	0.14	30.0	0.10	300.0
1.00E-02	5.00E-01	0.40	0.30	0.29	3.00	0.20	30.0	0.12	300.0
1.00E-02	1.00E-00	0.63	0.30	0.43	3.00	0.32	30.0	0.18	300.0
1.00E-02	2.00E-00	0.75	0.30	0.58	3.00	0.43	30.0	0.26	300.0
1.00E-02	5.00E-00	0.89	0.30	0.69	3.00	0.52	30.0	0.38	300.0
1.00E-02	1.00E+01	1.06	0.30	0.81	3.00	0.64	30.0	0.51	300.0
1.00E-02	2.00E+01	1.20	0.30	0.95	3.00	0.72	30.0	0.62	300.0
1.00E-02	5.00E+01	1.43	0.30	1.08	3.00	0.84	30.0	0.72	300.0
1.00E-02	1.00E+02	1.72	0.30	1.23	3.00	0.97	30.0	0.84	300.0
1.00E-02	2.00E+02	1.98	0.30	1.45	3.00	1.12	30.0	0.97	300.0
1.00E-02	5.00E+02	2.31	0.30	1.60	3.00	1.32	30.0	1.11	300.0
1.00E-02	1.00E+03	2.53	0.30	1.82	3.00	1.49	30.0	1.28	300.0
1.00E-02	2.00E+03	2.81	0.30	1.99	3.00	1.58	30.0	1.40	300.0
1.00E-02	5.00E+03	3.02	0.30	2.29	3.00	1.72	30.0	1.58	300.0
1.00E-02	1.00E+04	3.18	0.30	2.51	3.00	1.90	30.0	1.69	300.0
1.00E-02	2.00E+04	3.39	0.30	2.78	3.00	2.06	30.0	1.80	300.0
1.00E-02	5.00E+04	3.53	0.30	2.97	3.00	2.25	30.0	1.97	300.0
1.00E-02	1.00E+05	3.86	0.30	3.14	3.00	2.46	30.0	2.13	300.0
1.00E-02	2.00E+05	4.07	0.30	3.27	3.00	2.61	30.0	2.34	300.0
1.00E-02	5.00E+05	4.21	0.30	3.43	3.00	2.87	30.0	2.49	300.0
1.00E-02	1.00E+06	4.48	0.30	3.59	3.00	2.99	30.0	2.61	300.0

2.00E-02	1.00E-02	0.10	0.30	0.10	3.00	0.10	30.0	0.10	300.0
2.00E-02	2.00E-02	0.12	0.30	0.10	3.00	0.10	30.0	0.10	300.0
2.00E-02	5.00E-02	0.18	0.30	0.15	3.00	0.10	30.0	0.10	300.0
2.00E-02	1.00E-01	0.27	0.30	0.22	3.00	0.16	30.0	0.10	300.0
2.00E-02	2.00E-01	0.62	0.30	0.51	3.00	0.27	30.0	0.18	300.0
2.00E-02	5.00E-01	1.09	0.30	0.92	3.00	0.47	30.0	0.26	300.0
2.00E-02	1.00E-00	1.74	0.30	1.34	3.00	0.75	30.0	0.41	300.0
2.00E-02	2.00E-00	2.96	0.30	2.17	3.00	1.08	30.0	0.62	300.0
2.00E-02	5.00E-00	3.89	0.30	3.19	3.00	1.68	30.0	0.89	300.0
2.00E-02	1.00E+01	5.54	0.30	4.89	3.00	2.76	30.0	1.24	300.0
2.00E-02	2.00E+01	6.79	0.30	6.08	3.00	3.92	30.0	2.05	300.0
2.00E-02	5.00E+01	8.73	0.30	7.83	3.00	5.13	30.0	3.16	300.0
2.00E-02	1.00E+02	9.89	0.30	8.83	3.00	6.25	30.0	4.27	300.0
2.00E-02	2.00E+02	11.6	0.30	10.1	3.00	7.93	30.0	5.16	300.0
2.00E-02	5.00E+02	13.8	0.30	12.2	3.00	9.05	30.0	7.49	300.0
2.00E-02	1.00E+03	16.1	0.30	14.9	3.00	10.6	30.0	8.99	300.0
2.00E-02	2.00E+03	18.4	0.30	16.8	3.00	11.8	30.0	9.79	300.0
2.00E-02	5.00E+03	21.6	0.30	19.6	3.00	13.9	30.0	10.8	300.0
2.00E-02	1.00E+04	24.9	0.30	22.0	3.00	16.3	30.0	12.9	300.0
2.00E-02	2.00E+04	28.5	0.30	24.8	3.00	19.5	30.0	14.5	300.0
2.00E-02	5.00E+04	33.6	0.30	27.2	3.00	22.6	30.0	17.3	300.0
2.00E-02	1.00E+05	39.4	0.30	31.5	3.00	26.8	30.0	21.8	300.0
2.00E-02	2.00E+05	46.4	0.30	37.4	3.00	30.4	30.0	24.9	300.0
2.00E-02	5.00E+05	54.9	0.30	41.3	3.00	33.9	30.0	27.4	300.0
2.00E-02	1.00E+06	61.4	0.30	46.1	3.00	37.7	30.0	30.6	300.0
4.00E-02	1.00E-02	0.20	0.30	0.13	3.00	0.12	30.0	0.12	300.0
4.00E-02	2.00E-02	0.31	0.30	0.24	3.00	0.21	30.0	0.20	300.0
4.00E-02	5.00E-02	0.45	0.30	0.39	3.00	0.35	30.0	0.34	300.0
4.00E-02	1.00E-01	0.68	0.30	0.58	3.00	0.49	30.0	0.47	300.0
4.00E-02	2.00E-01	1.34	0.30	0.97	3.00	0.88	30.0	0.85	300.0
4.00E-02	5.00E-01	2.01	0.30	1.68	3.00	1.43	30.0	1.37	300.0
4.00E-02	1.00E-00	4.89	0.30	3.29	3.00	2.94	30.0	2.81	300.0
4.00E-02	2.00E-00	7.58	0.30	5.74	3.00	4.89	30.0	4.67	300.0
4.00E-02	5.00E-00	14.6	0.30	10.3	3.00	8.43	30.0	8.19	300.0
4.00E-02	1.00E+01	22.7	0.30	18.4	3.00	16.2	30.0	15.6	300.0
4.00E-02	2.00E+01	41.8	0.30	34.2	3.00	29.8	30.0	27.3	300.0
4.00E-02	5.00E+01	89.6	0.30	79.2	3.00	71.4	30.0	66.7	300.0
4.00E-02	1.00E+02	126	0.30	113	3.00	99.2	30.0	92.3	300.0
4.00E-02	2.00E+02	165	0.30	141	3.00	118	30.0	109	300.0
4.00E-02	5.00E+02	221	0.30	189	3.00	167	30.0	156	300.0
4.00E-02	1.00E+03	356	0.30	247	3.00	223	30.0	189	300.0
4.00E-02	2.00E+03	427	0.30	302	3.00	289	30.0	208	300.0
4.00E-02	5.00E+03	518	0.30	429	3.00	347	30.0	229	300.0
4.00E-02	1.00E+04	672	0.30	549	3.00	435	30.0	245	300.0
4.00E-02	2.00E+04	738	0.30	628	3.00	518	30.0	267	300.0
4.00E-02	5.00E+04	853	0.30	715	3.00	623	30.0	299	300.0
4.00E-02	1.00E+05	973	0.30	825	3.00	713	30.0	343	300.0
4.00E-02	2.00E+05	1093	0.30	936	3.00	784	30.0	384	300.0
4.00E-02	5.00E+05	1234	0.30	1024	3.00	825	30.0	426	300.0
4.00E-02	1.00E+06	1959	0.30	1139	3.00	889	30.0	487	300.0

7.00E-02	1.00E-02	0.19	0.30	0.12	3.00	0.11	30.0	0.11	300.0
7.00E-02	2.00E-02	0.30	0.30	0.23	3.00	0.20	30.0	0.19	300.0
7.00E-02	5.00E-02	0.43	0.30	0.37	3.00	0.34	30.0	0.32	300.0
7.00E-02	1.00E-01	0.66	0.30	0.55	3.00	0.46	30.0	0.45	300.0
7.00E-02	2.00E-01	1.30	0.30	0.91	3.00	0.83	30.0	0.80	300.0
7.00E-02	5.00E-01	1.95	0.30	1.60	3.00	1.38	30.0	1.30	300.0
7.00E-02	1.00E-00	4.80	0.30	3.12	3.00	2.83	30.0	2.67	300.0
7.00E-02	2.00E-00	7.43	0.30	5.63	3.00	4.72	30.0	4.54	300.0
7.00E-02	5.00E-00	14.2	0.30	10.0	3.00	8.30	30.0	8.01	300.0
7.00E-02	1.00E+01	21.2	0.30	17.9	3.00	15.7	30.0	14.3	300.0
7.00E-02	2.00E+01	38.8	0.30	33.4	3.00	28.1	30.0	24.8	300.0
7.00E-02	5.00E+01	84.6	0.30	74.2	3.00	68.3	30.0	61.3	300.0
7.00E-02	1.00E+02	119	0.30	106	3.00	91.3	30.0	84.3	300.0
7.00E-02	2.00E+02	155	0.30	131	3.00	105	30.0	98.5	300.0
7.00E-02	5.00E+02	211	0.30	171	3.00	154	30.0	140	300.0
7.00E-02	1.00E+03	345	0.30	233	3.00	206	30.0	168	300.0
7.00E-02	2.00E+03	413	0.30	291	3.00	270	30.0	191	300.0
7.00E-02	5.00E+03	505	0.30	402	3.00	325	30.0	202	300.0
7.00E-02	1.00E+04	661	0.30	519	3.00	409	30.0	223	300.0
7.00E-02	2.00E+04	722	0.30	601	3.00	489	30.0	241	300.0
7.00E-02	5.00E+04	840	0.30	691	3.00	600	30.0	247	300.0
7.00E-02	1.00E+05	951	0.30	799	3.00	682	30.0	302	300.0
7.00E-02	2.00E+05	1033	0.30	888	3.00	741	30.0	325	300.0
7.00E-02	5.00E+05	1147	0.30	936	3.00	779	30.0	379	300.0
7.00E-02	1.00E+06	1822	0.30	1041	3.00	821	30.0	411	300.0

1.00E-01	1.00E-02	0.18	0.30	0.12	3.00	0.13	30.0	0.13	300.0
1.00E-01	2.00E-02	0.28	0.30	0.22	3.00	0.22	30.0	0.21	300.0
1.00E-01	5.00E-02	0.41	0.30	0.35	3.00	0.34	30.0	0.32	300.0
1.00E-01	1.00E-01	0.62	0.30	0.51	3.00	0.44	30.0	0.45	300.0
1.00E-01	2.00E-01	1.25	0.30	0.87	3.00	0.77	30.0	0.78	300.0
1.00E-01	5.00E-01	1.87	0.30	1.51	3.00	1.23	30.0	1.25	300.0
1.00E-01	1.00E-00	4.69	0.30	2.97	3.00	2.62	30.0	2.53	300.0
1.00E-01	2.00E-00	7.31	0.30	5.43	3.00	4.47	30.0	4.38	300.0
1.00E-01	5.00E-00	14.0	0.30	9.51	3.00	7.89	30.0	7.71	300.0
1.00E-01	1.00E+01	20.3	0.30	16.8	3.00	13.7	30.0	13.2	300.0
1.00E-01	2.00E+01	37.1	0.30	32.0	3.00	24.1	30.0	20.1	300.0
1.00E-01	5.00E+01	82.8	0.30	72.5	3.00	64.2	30.0	52.8	300.0
1.00E-01	1.00E+02	108	0.30	97.4	3.00	80.1	30.0	70.2	300.0
1.00E-01	2.00E+02	143	0.30	106	3.00	91.2	30.0	84.2	300.0
1.00E-01	5.00E+02	200	0.30	153	3.00	120	30.0	115	300.0
1.00E-01	1.00E+03	321	0.30	201	3.00	153	30.0	142	300.0
1.00E-01	2.00E+03	398	0.30	242	3.00	198	30.0	165	300.0
1.00E-01	5.00E+03	468	0.30	337	3.00	251	30.0	189	300.0
1.00E-01	1.00E+04	587	0.30	428	3.00	301	30.0	201	300.0
1.00E-01	2.00E+04	659	0.30	506	3.00	389	30.0	233	300.0
1.00E-01	5.00E+04	726	0.30	596	3.00	462	30.0	250	300.0
1.00E-01	1.00E+05	812	0.30	684	3.00	538	30.0	289	300.0
1.00E-01	2.00E+05	915	0.30	792	3.00	597	30.0	315	300.0
1.00E-01	5.00E+05	1046	0.30	837	3.00	628	30.0	348	300.0
1.00E-01	1.00E+06	1247	0.30	904	3.00	706	30.0	399	300.0

2.00E-01	1.00E-02	0.19	0.30	0.13	3.00	0.11	30.0	0.11	300.0
2.00E-01	2.00E-02	0.29	0.30	0.23	3.00	0.20	30.0	0.19	300.0
2.00E-01	5.00E-02	0.42	0.30	0.35	3.00	0.33	30.0	0.31	300.0
2.00E-01	1.00E-01	0.62	0.30	0.51	3.00	0.43	30.0	0.44	300.0
2.00E-01	2.00E-01	1.24	0.30	0.86	3.00	0.77	30.0	0.77	300.0
2.00E-01	5.00E-01	1.86	0.30	1.48	3.00	1.23	30.0	1.25	300.0
2.00E-01	1.00E-00	4.65	0.30	2.84	3.00	2.65	30.0	2.54	300.0
2.00E-01	2.00E-00	7.24	0.30	5.25	3.00	4.52	30.0	4.41	300.0
2.00E-01	5.00E-00	13.5	0.30	9.08	3.00	8.01	30.0	7.82	300.0
2.00E-01	1.00E+01	29.1	0.30	15.3	3.00	14.9	30.0	13.7	300.0
2.00E-01	2.00E+01	35.0	0.30	28.8	3.00	26.8	30.0	20.9	300.0
2.00E-01	5.00E+01	77.3	0.30	67.9	3.00	64.2	30.0	55.2	300.0
2.00E-01	1.00E+02	100	0.30	90.1	3.00	86.3	30.0	75.3	300.0
2.00E-01	2.00E+02	131	0.30	98.7	3.00	99.6	30.0	89.2	300.0
2.00E-01	5.00E+02	182	0.30	134	3.00	139	30.0	124	300.0
2.00E-01	1.00E+03	293	0.30	174	3.00	169	30.0	148	300.0
2.00E-01	2.00E+03	337	0.30	216	3.00	211	30.0	167	300.0
2.00E-01	5.00E+03	438	0.30	313	3.00	274	30.0	187	300.0
2.00E-01	1.00E+04	546	0.30	401	3.00	338	30.0	201	300.0
2.00E-01	2.00E+04	614	0.30	479	3.00	418	30.0	213	300.0
2.00E-01	5.00E+04	672	0.30	527	3.00	493	30.0	220	300.0
2.00E-01	1.00E+05	738	0.30	618	3.00	579	30.0	279	300.0
2.00E-01	2.00E+05	857	0.30	706	3.00	628	30.0	305	300.0
2.00E-01	5.00E+05	927	0.30	773	3.00	681	30.0	338	300.0
2.00E-01	1.00E+06	1099	0.30	837	3.00	739	30.0	389	300.0
4.00E-01	1.00E-02	0.20	0.30	0.15	3.00	0.14	30.0	0.14	300.0
4.00E-01	2.00E-02	0.30	0.30	0.24	3.00	0.23	30.0	0.22	300.0
4.00E-01	5.00E-02	0.44	0.30	0.36	3.00	0.35	30.0	0.33	300.0
4.00E-01	1.00E-01	0.64	0.30	0.51	3.00	0.45	30.0	0.46	300.0
4.00E-01	2.00E-01	1.25	0.30	0.86	3.00	0.78	30.0	0.78	300.0
4.00E-01	5.00E-01	1.87	0.30	1.47	3.00	1.23	30.0	1.26	300.0
4.00E-01	1.00E-00	4.65	0.30	2.82	3.00	2.65	30.0	2.54	300.0
4.00E-01	2.00E-00	7.23	0.30	5.21	3.00	4.48	30.0	4.40	300.0
4.00E-01	5.00E-00	13.4	0.30	9.01	3.00	7.91	30.0	7.76	300.0
4.00E-01	1.00E+01	29.0	0.30	15.2	3.00	14.7	30.0	13.3	300.0
4.00E-01	2.00E+01	34.2	0.30	28.6	3.00	26.2	30.0	20.1	300.0
4.00E-01	5.00E+01	76.7	0.30	67.2	3.00	63.5	30.0	53.7	300.0
4.00E-01	1.00E+02	98.6	0.30	89.0	3.00	85.1	30.0	74.2	300.0
4.00E-01	2.00E+02	127	0.30	94.2	3.00	98.3	30.0	87.1	300.0
4.00E-01	5.00E+02	177	0.30	128	3.00	129	30.0	119	300.0
4.00E-01	1.00E+03	288	0.30	168	3.00	160	30.0	143	300.0
4.00E-01	2.00E+03	330	0.30	209	3.00	198	30.0	154	300.0
4.00E-01	5.00E+03	426	0.30	301	3.00	260	30.0	176	300.0
4.00E-01	1.00E+04	527	0.30	389	3.00	321	30.0	189	300.0
4.00E-01	2.00E+04	597	0.30	463	3.00	402	30.0	201	300.0
4.00E-01	5.00E+04	642	0.30	516	3.00	476	30.0	210	300.0
4.00E-01	1.00E+05	711	0.30	605	3.00	561	30.0	263	300.0
4.00E-01	2.00E+05	831	0.30	691	3.00	605	30.0	292	300.0
4.00E-01	5.00E+05	889	0.30	758	3.00	667	30.0	321	300.0
4.00E-01	1.00E+06	1010	0.30	819	3.00	724	30.0	376	300.0

7.00E-01	1.00E-02	0.23	0.30	0.16	3.00	0.15	30.0	0.15	300.0
7.00E-01	2.00E-02	0.33	0.30	0.26	3.00	0.24	30.0	0.24	300.0
7.00E-01	5.00E-02	0.47	0.30	0.38	3.00	0.37	30.0	0.35	300.0
7.00E-01	1.00E-01	0.66	0.30	0.53	3.00	0.46	30.0	0.47	300.0
7.00E-01	2.00E-01	1.28	0.30	0.88	3.00	0.79	30.0	0.79	300.0
7.00E-01	5.00E-01	1.89	0.30	1.49	3.00	1.24	30.0	1.26	300.0
7.00E-01	1.00E-00	4.70	0.30	2.84	3.00	2.66	30.0	2.55	300.0
7.00E-01	2.00E-00	7.25	0.30	5.25	3.00	4.52	30.0	4.41	300.0
7.00E-01	5.00E-00	13.4	0.30	9.00	3.00	8.01	30.0	7.82	300.0
7.00E-01	1.00E+01	29.0	0.30	15.2	3.00	14.7	30.0	13.4	300.0
7.00E-01	2.00E+01	34.1	0.30	28.2	3.00	26.1	30.0	20.1	300.0
7.00E-01	5.00E+01	76.6	0.30	67.0	3.00	62.1	30.0	53.9	300.0
7.00E-01	1.00E+02	98.1	0.30	88.1	3.00	84.0	30.0	72.4	300.0
7.00E-01	2.00E+02	123	0.30	96.1	3.00	93.3	30.0	85.1	300.0
7.00E-01	5.00E+02	173	0.30	128	3.00	122	30.0	118	300.0
7.00E-01	1.00E+03	281	0.30	163	3.00	152	30.0	139	300.0
7.00E-01	2.00E+03	322	0.30	207	3.00	198	30.0	154	300.0
7.00E-01	5.00E+03	418	0.30	302	3.00	259	30.0	163	300.0
7.00E-01	1.00E+04	519	0.30	390	3.00	320	30.0	189	300.0
7.00E-01	2.00E+04	584	0.30	460	3.00	399	30.0	195	300.0
7.00E-01	5.00E+04	631	0.30	509	3.00	471	30.0	203	300.0
7.00E-01	1.00E+05	700	0.30	604	3.00	560	30.0	261	300.0
7.00E-01	2.00E+05	819	0.30	691	3.00	604	30.0	289	300.0
7.00E-01	5.00E+05	877	0.30	750	3.00	662	30.0	320	300.0
7.00E-01	1.00E+06	996	0.30	819	3.00	719	30.0	358	300.0
1.00E-00	1.00E-02	0.26	0.30	0.19	3.00	0.18	30.0	0.17	300.0
1.00E-00	2.00E-02	0.36	0.30	0.29	3.00	0.27	30.0	0.26	300.0
1.00E-00	5.00E-02	0.48	0.30	0.40	3.00	0.38	30.0	0.37	300.0
1.00E-00	1.00E-01	0.69	0.30	0.54	3.00	0.47	30.0	0.45	300.0
1.00E-00	2.00E-01	1.29	0.30	0.89	3.00	0.79	30.0	0.72	300.0
1.00E-00	5.00E-01	1.89	0.30	1.49	3.00	1.22	30.0	1.18	300.0
1.00E-00	1.00E-00	4.69	0.30	2.83	3.00	2.60	30.0	2.48	300.0
1.00E-00	2.00E-00	7.21	0.30	5.18	3.00	4.41	30.0	4.34	300.0
1.00E-00	5.00E-00	13.2	0.30	8.89	3.00	7.87	30.0	7.71	300.0
1.00E-00	1.00E+01	28.2	0.30	13.9	3.00	14.0	30.0	12.4	300.0
1.00E-00	2.00E+01	33.0	0.30	26.1	3.00	24.5	30.0	18.8	300.0
1.00E-00	5.00E+01	73.2	0.30	65.1	3.00	59.9	30.0	50.1	300.0
1.00E-00	1.00E+02	96.1	0.30	85.3	3.00	81.6	30.0	69.3	300.0
1.00E-00	2.00E+02	118	0.30	93.7	3.00	90.7	30.0	82.7	300.0
1.00E-00	5.00E+02	165	0.30	120	3.00	115	30.0	108	300.0
1.00E-00	1.00E+03	263	0.30	151	3.00	146	30.0	121	300.0
1.00E-00	2.00E+03	306	0.30	198	3.00	190	30.0	131	300.0
1.00E-00	5.00E+03	401	0.30	290	3.00	244	30.0	148	300.0
1.00E-00	1.00E+04	502	0.30	371	3.00	303	30.0	170	300.0
1.00E-00	2.00E+04	563	0.30	441	3.00	380	30.0	181	300.0
1.00E-00	5.00E+04	610	0.30	490	3.00	458	30.0	188	300.0
1.00E-00	1.00E+05	685	0.30	588	3.00	537	30.0	247	300.0
1.00E-00	2.00E+05	800	0.30	667	3.00	588	30.0	262	300.0
1.00E-00	5.00E+05	856	0.30	729	3.00	649	30.0	292	300.0
1.00E-00	1.00E+06	980	0.30	802	3.00	700	30.0	323	300.0

2.00E-00	1.00E-02	0.32	0.30	0.25	3.00	0.24	30.0	0.22	300.0
2.00E-00	2.00E-02	0.39	0.30	0.34	3.00	0.32	30.0	0.30	300.0
2.00E-00	5.00E-02	0.53	0.30	0.44	3.00	0.42	30.0	0.40	300.0
2.00E-00	1.00E-01	0.72	0.30	0.58	3.00	0.51	30.0	0.48	300.0
2.00E-00	2.00E-01	1.31	0.30	0.92	3.00	0.82	30.0	0.74	300.0
2.00E-00	5.00E-01	1.90	0.30	1.51	3.00	1.25	30.0	1.19	300.0
2.00E-00	1.00E-00	4.70	0.30	2.84	3.00	2.62	30.0	2.48	300.0
2.00E-00	2.00E-00	7.21	0.30	5.18	3.00	4.42	30.0	4.34	300.0
2.00E-00	5.00E-00	13.2	0.30	8.89	3.00	7.87	30.0	7.61	300.0
2.00E-00	1.00E+01	28.1	0.30	13.8	3.00	13.1	30.0	12.0	300.0
2.00E-00	2.00E+01	32.0	0.30	25.9	3.00	24.0	30.0	17.1	300.0
2.00E-00	5.00E+01	70.1	0.30	63.2	3.00	57.1	30.0	47.9	300.0
2.00E-00	1.00E+02	93.1	0.30	82.5	3.00	77.9	30.0	66.1	300.0
2.00E-00	2.00E+02	113	0.30	90.2	3.00	87.1	30.0	79.2	300.0
2.00E-00	5.00E+02	158	0.30	115	3.00	109	30.0	101	300.0
2.00E-00	1.00E+03	257	0.30	141	3.00	135	30.0	110	300.0
2.00E-00	2.00E+03	298	0.30	187	3.00	173	30.0	120	300.0
2.00E-00	5.00E+03	391	0.30	278	3.00	227	30.0	126	300.0
2.00E-00	1.00E+04	489	0.30	357	3.00	289	30.0	156	300.0
2.00E-00	2.00E+04	550	0.30	426	3.00	361	30.0	163	300.0
2.00E-00	5.00E+04	588	0.30	470	3.00	435	30.0	173	300.0
2.00E-00	1.00E+05	670	0.30	569	3.00	520	30.0	222	300.0
2.00E-00	2.00E+05	781	0.30	651	3.00	561	30.0	249	300.0
2.00E-00	5.00E+05	832	0.30	708	3.00	632	30.0	270	300.0
2.00E-00	1.00E+06	958	0.30	789	3.00	688	30.0	301	300.0
3.00E-00	1.00E-02	0.37	0.30	0.31	3.00	0.29	30.0	0.27	300.0
3.00E-00	2.00E-02	0.44	0.30	0.38	3.00	0.34	30.0	0.32	300.0
3.00E-00	5.00E-02	0.59	0.30	0.48	3.00	0.44	30.0	0.42	300.0
3.00E-00	1.00E-01	0.76	0.30	0.61	3.00	0.53	30.0	0.50	300.0
3.00E-00	2.00E-01	1.33	0.30	0.94	3.00	0.83	30.0	0.76	300.0
3.00E-00	5.00E-01	1.92	0.30	1.53	3.00	1.26	30.0	1.20	300.0
3.00E-00	1.00E-00	4.71	0.30	2.85	3.00	2.63	30.0	2.49	300.0
3.00E-00	2.00E-00	7.21	0.30	5.18	3.00	4.42	30.0	4.34	300.0
3.00E-00	5.00E-00	13.2	0.30	8.89	3.00	7.87	30.0	7.55	300.0
3.00E-00	1.00E+01	28.0	0.30	13.2	3.00	12.3	30.0	11.2	300.0
3.00E-00	2.00E+01	30.1	0.30	24.0	3.00	22.1	30.0	15.7	300.0
3.00E-00	5.00E+01	67.9	0.30	60.1	3.00	55.0	30.0	44.1	300.0
3.00E-00	1.00E+02	90.0	0.30	79.2	3.00	74.2	30.0	62.3	300.0
3.00E-00	2.00E+02	106	0.30	87.1	3.00	83.8	30.0	75.7	300.0
3.00E-00	5.00E+02	148	0.30	108	3.00	101	30.0	95.9	300.0
3.00E-00	1.00E+03	241	0.30	130	3.00	123	30.0	102	300.0
3.00E-00	2.00E+03	280	0.30	171	3.00	160	30.0	110	300.0
3.00E-00	5.00E+03	371	0.30	265	3.00	210	30.0	119	300.0
3.00E-00	1.00E+04	473	0.30	341	3.00	272	30.0	145	300.0
3.00E-00	2.00E+04	533	0.30	407	3.00	349	30.0	155	300.0
3.00E-00	5.00E+04	572	0.30	451	3.00	419	30.0	163	300.0
3.00E-00	1.00E+05	653	0.30	550	3.00	501	30.0	201	300.0
3.00E-00	2.00E+05	767	0.30	635	3.00	548	30.0	232	300.0
3.00E-00	5.00E+05	818	0.30	689	3.00	611	30.0	252	300.0
3.00E-00	1.00E+06	940	0.30	770	3.00	667	30.0	280	300.0

^a In $M_{\odot} \text{ yr}^{-1}$.

^b The notation aEb denotes $a \times 10^b$.

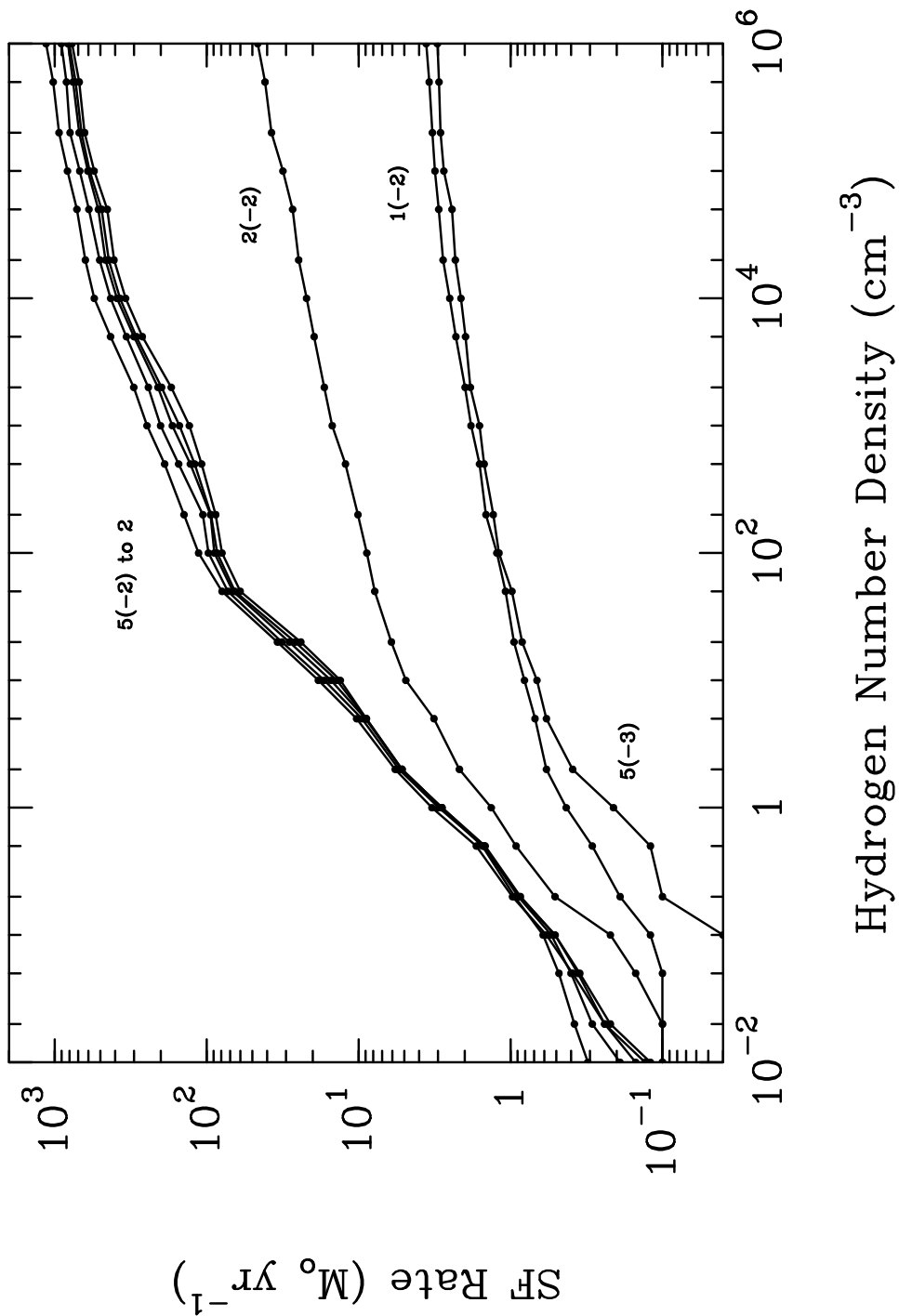


Fig. 1.— The star formation rate as a function of hydrogen number density, for various metallicities, a total mass of M_g and a background star formation rate of $S_b = 3 M_{\odot} \text{ yr}^{-1}$. The various curves are labelled by the ambient metallicity relative to Solar.

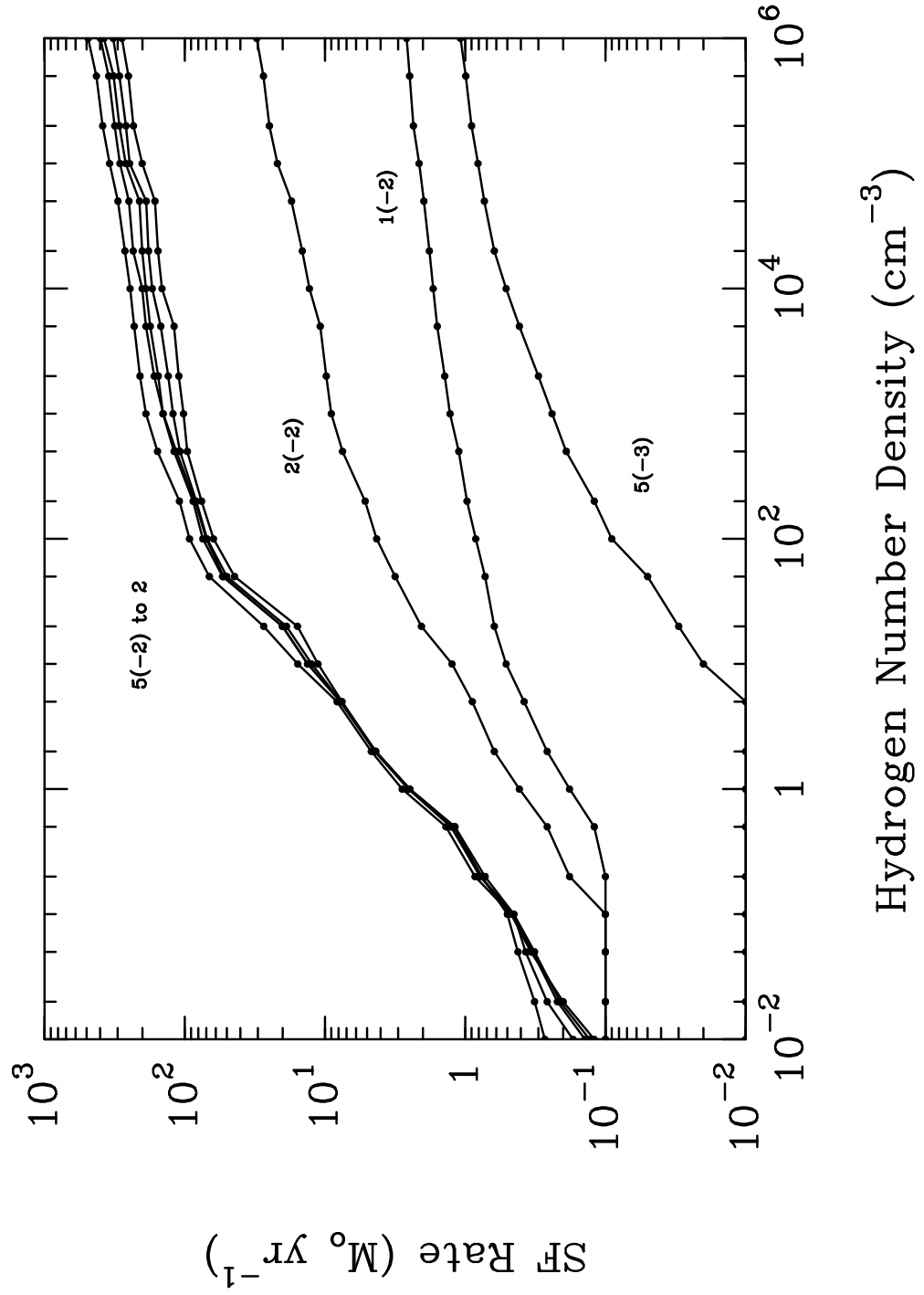


Fig. 2.— Same as Figure 1, for $S_b = 300 M_{\odot} \text{ yr}^{-1}$.